| | |
|---|---|
| **Preprint Title** | Deterministic Model of Observed Colours on Metal-Anodic Aluminium Oxide-Al Nanostructures |
| **Authors** | Cristina V. Manzano, Jakob J. Schwiedrzik, Gerhard Bürki, Laszlo Pethö, Johann Michler and Laetitia Philippe |
| **Publication Date** | 09 Jan 2020 |
| **Article Type** | Full Research Paper |
| **Supporting Information File 1** | Supporting information Deterministic Model of Observed Colours on 09.01.2020.docx; 4.6 MB |
| **ORCID® iDs** | Cristina V. Manzano - https://orcid.org/0000-0001-5708-6544 |

# Deterministic Model of Observed Colours on Metal-Anodic Aluminium Oxide-Al Nanostructures

Cristina V. Manzano[1,*], Jakob J. Schwiedrzik[1], Gerhard Bürki[1], Laszlo Pethö[1], Johann Michler[1], Laetitia Philippe[1]

[1] *Empa, Swiss Federal Laboratories for Materials Science and Technology, Laboratory for Mechanics of Materials and Nanostructures, Feuerwerkerstrasse 39, CH-3602 Thun, Switzerland*

## Abstract

Structural colours have produced immense attention in reproducing the vivid colours found in nature. In this study, metal-anodic aluminium oxide (AAO)-Al nanostructures were deposited using a two-step anodization and sputtering process to produce self-ordered anodic aluminium oxide films and a metal layer (8 nm Cr and 25,17.5 and 10 nm of Au), respectively. AAO films, of various thicknesses, were anodized and the *Yxy* values (*Y*, luminance, and *xy*, chromaticity) were obtained via reflectance measurements. An empirical model, based on the thickness and porosity of the nanostructures, was determined, which would describe a gamut of colours. The proposed mathematical model can be applied in different fields, such as wavelength absorbers, RGB (red, green, blue) display devices, as well as chemical or optical sensors.

**Keywords:** Anodic aluminium oxide (AAO) films, anodization, reflectance, polar coordinate, plasmonic, colours

## Introduction

In recent times, the development of brilliant colours has produced immense interest in reproducing the vivid colours found in nature[1]. These colours appear when light interacts with periodic structures. For this purpose, anodic aluminium oxide films play an important role. There are different approaches in obtaining brilliant colours using AAO films, such as using new anodization electrolytes (etidronic acid)[2], via pulsed anodization[3], as well as by depositing a metal layer onto the surface of AAO-Al films[4]. Specifically, metal-AAO-Al nanostructures exhibit structural colours, which can find applications as wavelength absorbers[5], RGB display devices[6] and chemical[7] or optical sensors[8]. In this sense, it is essential to develop a model, which would allow to determine the colours (RGB or *Yxy* values of CIElab 1931) obtained by these nanostructures based on the morphological parameters of the AAO films.

The colour observed in metal-AAO-Al nanostructures depends on the morphological parameters of the AAO films and on the metal's nature and thickness once deposited onto the AAO-Al films. In a previous study by our group, the effects of morphological parameters (pore diameters, interpore distance, porosity, nanostructure order) on the colours and the effective refractive index of AAO films were studied on metal-AAO-Al nanostructures[4]. Thickness and porosity are the two main structural parameters, which affect the observed colours and effective refractive index of the AAO films. By tuning either one of those parameters, or by changing the nature of the coating, it is possible to obtain the entire visible spectrum. In literature, different studies can be found, where the colour is changed by changing the used metal (Pt/Pd, Al, Cr, Ag, Au)[9, 10], carbon[5] or by changing the thickness of the metal [9, 11, 12].

There are two published studies, where wavelength values were generated [13, 14] by using a model which could predict colours by taking into account the morphological parameters of AAO films and the deposited metal layer. One put forward an equation to determine the thickness of the AAO layer, which would create strong absorption at a given wavelength[13]. The other work proposed an empirical equation, which would be able to design colours by pre-setting the specific thickness also through wavelengths[14]. As humans are trichromatic, the retina contains three types of colour receptor cells, also known as cones: a) S cones, short-wavelength cones or blue cones; b) M cones, middle-wavelength cones or green cones and c) L cones, long-wavelength cones or red cones, where a full plot of all visible colour is a 3D Figure [15]. CIElab colour space was created by the International Commission on Illumination

(CIE) in 1931[12] in order to determine a colour model, which would be perpetually uniform with respect to the human colour vision. This model can be described as RGB colour space or *Yxy* colour space. For this reason, it is important to put forward a model, which would describe a wide range of colours using not only wavelengths, but also tristimulus values. To date, a model to estimate the colours using RGB values or *Yxy* values from reflectance measurements and morphological properties (thickness and porosity) has not been defined.

The purpose of this work is to obtain an empirical model to estimate a gamut of colours knowing only the thickness and porosity of the AAO films. The model was developed using *Yxy* values measuring only the reflectance, thickness and porosity of the films defined by means of SEM. To achieve this, AAO films of varying thicknesses were anodized and the obtained *Yxy* values were converted into polar coordinates to determine the relationship between the thickness and the colour range described by the *xy* values. Additionally, the *xy* equations are written in terms of effective refractive index and second anodization time, as there is a dependency between the thickness of AAO films and the effective refractive index, as well as the duration of the second anodization process. The model proposed in this study was defined for two different metals, chromium and gold. The work reported in this manuscript provides a mathematical model to estimate the *xy* values, colour diagram CIElab 1931, by only measuring the thickness and porosity of the AAO films.

## Results and discussion

### *AAO film surface morphology*

As was mentioned in the introduction, thickness and porosity are the two morphological parameters of AAO films that have the greatest influence on the colour obtained when depositing a metal layer on top of these nanostructures. Different AAO films were anodized under the same conditions (same porosity), changing only the second anodization time (from 120 to 600 s) to obtain different thicknesses (209 ± 12 nm to 380 ± 15 nm). FIB milling and FE-SEM imaging were used to accurately determine the films' thickness, as was done in a previous study[4]. The porosity, *P*, of the AAO templates is given by the following equation:

$$P = \frac{2\pi}{\sqrt{3}}\left(\frac{D_P/2}{D_{int}}\right)^2 \quad (1)$$

where: $D_p$ – pore diameter, $D_{int}$ – interpore distance.[16] The porosity values were found to be 8.3 %, 8.1 % and 7.3 % for AAO-Al films, 8 nm for Cr-AAO-Al films and 10 nm for Au-AAO-Al films, respectively (see Figure 1).

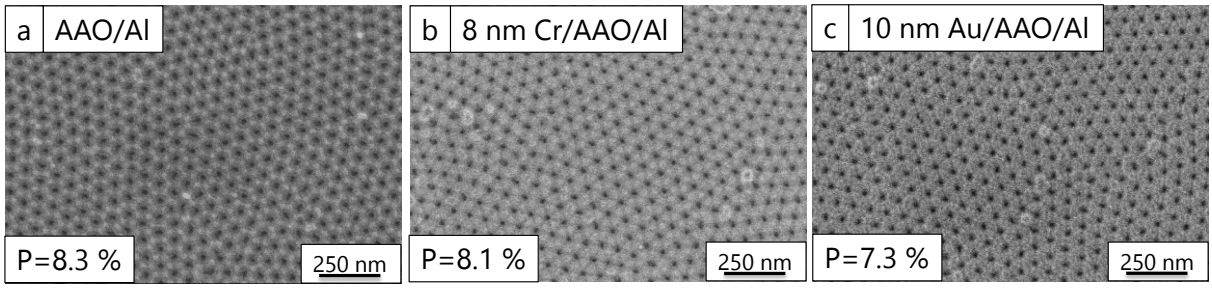


Figure 1. (a) FE-SEM images of AAO-Al films, (b) FE-SEM images of 8 nm Cr-AAO-Al films and (c) FE-SEM images of 10 nm Au-AAO-Al films.

As was expected, the porosity of the nanostructures on the surface was smaller after deposition (Cr and Au), where the smallest value, was achieved for 10 nm Au. It can be concluded that the nanoparticle's size is bigger for 10 nm Au than for 8 nm Cr. The colour obtained by both metals will vary depending on the thickness of the AAO films, as a result of porosity changes. Figure S1 (supporting information) shows FE-SEM images of AAO-Al films, reflectance before and after the deposition of 25 nm of Au, and the colour diagram of these nanostructures with different porosity volume fractions (9, 26, 31 and 41%). A change in the obtained reflectance and colour is observed for different porosity values. It can be concluded from the reflectance spectra (Figure S1e) that with the increase in porosity, a blue-shift is observed. With respect to the colour diagram (Figure S1f), as the porosity increases, the colours turn counter-clockwise.

*Reflectance, colour diagram and xy values of 8 nm Cr-AAO-Al and 10 nm Au-AAO-Al nanostructures*

UV-Vis reflection spectra of AAO films with different thicknesses for AAO-Al films, for 8 nm Cr-AAO-Al films and for 10 nm Au-AAO-Al films are shown in Figure 2a, 2b and 2c, respectively.

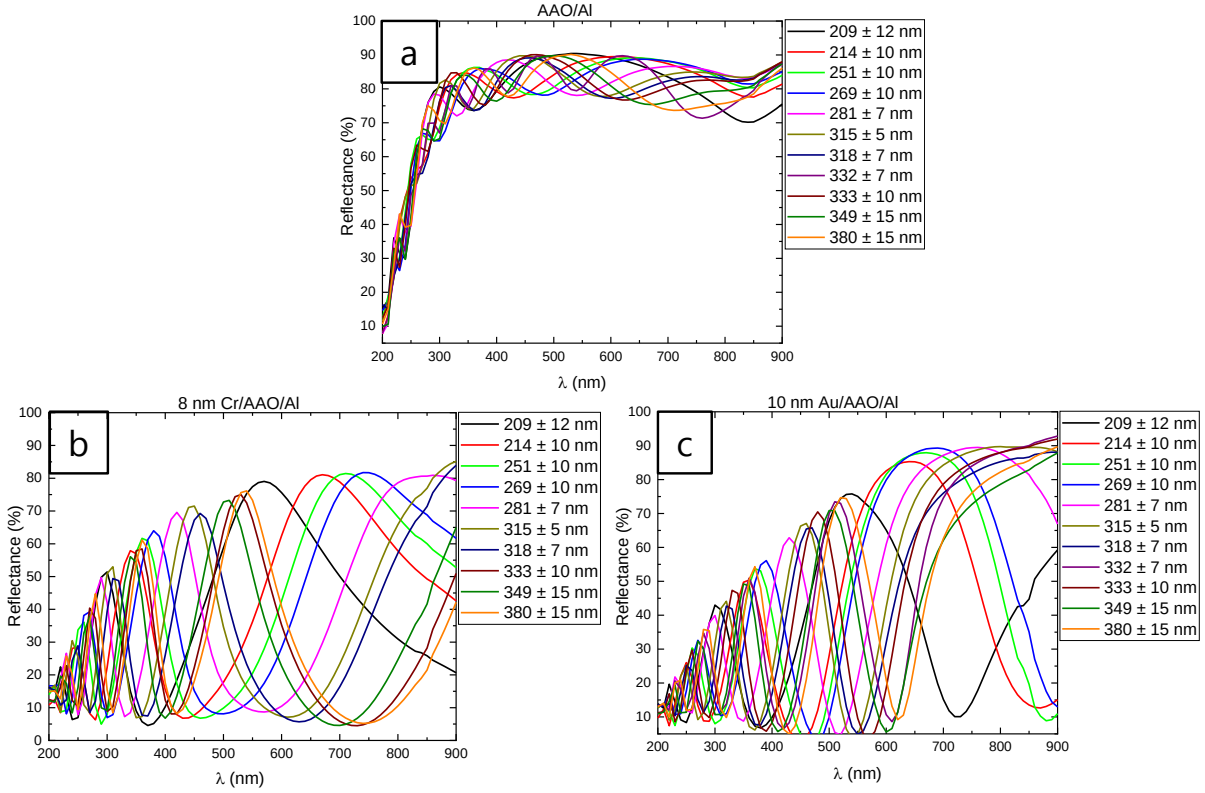


Figure 2. (a) UV-Vis reflectance spectra for AAO-Al films, (b) UV-Vis reflectance spectra for 8 nm Cr-AAO-Al films and (c) UV-Vis reflectance spectra for 10 nm Au-AAO-Al films with different thicknesses.

As shown in Figure 2a, the number of fringes increases with the increase in thickness. For the same number of fringes, a red-shift is observed when the thickness increases. This behaviour has already been observed in literature.[17, 18] In both cases, after the deposition of 8 nm of Cr and 10 nm of Au on top of the AAO-Al films (see Figure 2b and 2c), a blue-shift and a decrease in the reflectance is observed, due to plasmonic effects[4, 11, 13]. The wavelength of each sample and consequently the colour that the films will exhibit can be obtained from the maximum reflectance. The observed colours, the maximum reflectance wavelengths and colours from these wavelengths for each thickness are presented in Table 1.

Table 1. AAO thickness, observed colour, wavelength of maximum reflectance and colour obtained from the wavelength for 8 nm Cr/AAO/Al and 10 nm Au/AAO/Al nanostructures.

| **8 nm Cr/AAO/Al nanostructures** | | | |
|---|---|---|---|
| Thickness (nm) | Colour observed | $\lambda_{max}$(nm) | Colour from $\lambda_{max}$ |
| 209 ± 12 | Yellow | 569 | Yellow |
| 214 ± 10 | Orange | 671 | Red |
| 251 ± 10 | Orange | 708 | Red |
| 269 ± 10 | Pink | 700 | Red |
| 281 ± 7 | Violet | 420 | Violet |
| 315 ± 5 | Blue | 450 | Blue |

| | | | |
|---|---|---|---|
| 318 ± 7 | Blue-green | 460 | Blue |
| 333 ± 10 | Green | 530 | Green |
| 349 ± 15 | Green | 509 | Green |
| 380 ± 15 | Green | 540 | Green |
| **10 nm Au/AAO/Al nanostructures** | | | |
| Thickness (nm) | Colour observed | $\lambda_{max}$(nm) | Colour from $\lambda_{max}$ |
| 209 ± 12 | Yellow | 536 | Green |
| 214 ± 10 | Orange | 645 | Red |
| 251 ± 10 | Orange | 667 | Red |
| 269 ± 10 | Orange | 681 | Red |
| 281 ± 7 | Pink | 748 | Red |
| 315 ± 5 | Pink | 458 | Blue |
| 318 ± 7 | Blue | 483 | Blue-green |
| 332 ± 7 | Green | 509 | Green |
| 333 ± 10 | Green | 511 | Green |
| 349 ± 15 | Green | 507 | Green |
| 380 ± 15 | Green | 523 | Green |

As can be seen in Table 1, the colours obtained from the wavelength and the observed colour are not the same for certain thicknesses. Therefore, the wavelength should not be the only parameter taken into consideration when designing a model for predicting colours. As was mentioned in the introduction, humans are trichromatic. The CIElab colour space describes the RGB colour space or *Yxy* colour space for the entire gamut of colours using tristimulus values. For colour prediction it is necessary to obtain either *Yxy* values or RGB values. The *Yxy* values were calculated from the reflectance spectra of the AAO-Al, 8 nm Cr-AAO-Al and 10, 17.5 and 25 nm Au-AAO-Al nanostructures using the CIE 1931 colour space. The concept of colour can be divided into two parts, brightness and chromaticity, where *Y* is luminance, which defines brightness, and *x* and *y* are values that define chromaticity. It is possible to determine the gamut of human vision by only considering the *x* and *y* values.

Figure 3a shows the colour coordinates in the CIE 1931 colour diagram for Cr and Au with different thicknesses. Different colours, i.e. *xy* values, were obtained for Cr and Au, as well as for the different Au thicknesses. It should be noted that in this Figure more Metal-AAO-Al films (from 209 ± 12 nm to 951 ± 19 nm) are presented in order to show the change of *x* and *y* values when different Au thicknesses are sputtered on AAO-Al films. However, the colour model was designed only with AAO films with the thickness in the range of 209 ± 12 nm to 380 ± 15 nm, as a complete circle in the colour diagram is covered. For thicker samples, more circles are included within the inner part of the colour diagram.

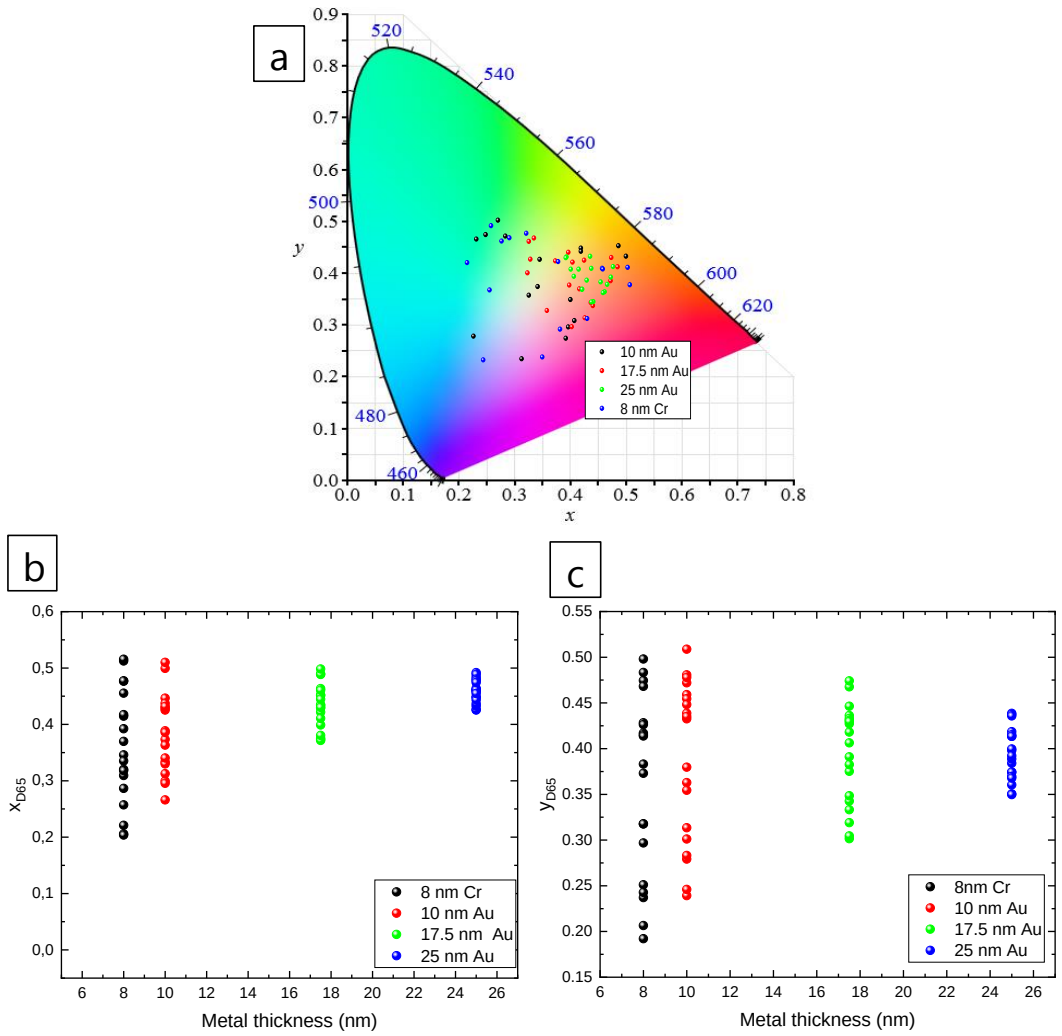


Figure 3. (a) Representation of CIE 1931colour diagram for different metals (Cr, 8nm, and Au) and different Au thicknesses (10, 17.5 and 25 nm). (b) *x*, (c) *y* as function of metal thickness.

As is observed in Figure 3, 17.5 nm Au and 25 nm Au do not display a large colour range (*x* and *y* values). For this reason, the colour model was created using 8 nm Cr and 10 nm Au on top of the AAO-Al nanostructures. The thickness and *x* and *y* values for both samples are presented in Table S1.

*Empirical model to obtain the colours observed in Cr/Au-AAO-Al nanostructures*

An empirical model was defined by using the thickness values measured from SEM images and *x* and *y* values obtained from the reflectance measurements. The proposed model defines a spiral shape. First, Cartesian coordinates (*x*,*y*) are transformed to polar coordinates (r, θ) by applying the equations collected in the supporting information ((S1) and (S2)). The values

were divided into two different ranges, as the nanostructures' *x* and *y* coordinates lie very far from each other on the colour diagram for thicknesses between 209-332 nm and 332-380 nm, even when the AAO films have very similar thicknesses (see Figure 4). The equations obtained for 8 nm Cr/AAO/Al nanostructures are:

$$x_{Cr,209\text{-}332nm}(\theta) = R(\theta)\cdot\cos\theta + 0.3137$$

$$y_{Cr,209\text{-}332nm}(\theta) = R(\theta)\cdot\sin\theta + 0.3664 \quad (2)$$

where $\theta_{Cr,209\text{-}332nm}(d) = -(0.36\pm0.06)\cdot10^{-1}\cdot d + (8.75\pm1.57)$ with $R^2=0.88$

and $R(\theta) = -(0.11\pm0.82)\cdot10^{-1}\cdot\theta + (0.15\pm0.01)$ for $209<d<332$ nm

and

$$x_{Cr,333\text{-}380nm}(\theta) = R(\theta)\cdot\cos\theta + 0.4631$$

$$y_{Cr,333\text{-}380nm}(\theta) = R(\theta)\cdot\sin\theta + 0.3343 \quad (3)$$

where $\theta_{Cr,333\text{-}380nm}(d) = (0.74\pm0.20)\cdot10^{-1}\cdot d - (27.71\pm7.74)$ with $R^2=0.56$

and $R(\theta)=(0.34\pm0.31)\cdot10^{-2}\cdot\theta + (0.21\pm0.07)\cdot10^{-1}$ for $333<d<380$ nm

where *d* is the thickness.

The equations obtained for 10 nm Au/AAO/Al nanostructures are shown in the supporting information ((S3) and (S4)). Note that these equations are valid when AAO-Al films have a porosity of 8.3 %. Equations (2)/(3) and (S3)/(S4) are very similar, as the top pore diameter after the deposition of 8 nm Cr (8.1%) and after 10 nm Au (7.3 %) is similar and the colours (*x* and *y* values) obtained after the metal deposition process are comparable (see Figure 4 and Table S1).

In a previous study carried out by our group, the dependence of effective refractive index and the thickness of AAO films for different anodization electrolytes was obtained[4]. In this work, more films and thinner films were studied, therefore it is necessary to recalculate the equation for the thickness range 209 ± 12 nm to 951 ± 19 nm. An exponential equation was obtained (see Figure S2 of the supporting information):

$$n_{eff} = (4.12 \pm 1.07)\cdot e^{\left(\frac{d}{183.84\pm52.50}\right)} + (1.64 \pm 0.19) \quad (4)$$

The dependency between the effective refractive index and the thickness obtained in the previous study [4] was linear, as the thickness of the AAO films varied between approx. 400 to 1300 nm. Moreover, the thickness can be formulated as a function of the second anodization time, as shown below:

$$d = (54.23 \pm 1.43) \cdot t^{2nd} + (90.03 \pm 9.31) \quad (5)$$

The relationship between the thickness of AAO films and the second anodization time is linear (see Figure S3 of the supporting information). The equations for 8 nm Cr/AAO/Al and 10 nm Au/AAO/Al nanostructures can now be written as a function of the effective refractive index and second anodization time, as can be found in the supporting information, from (S5) to (S8).

Figure 4a and 4b show the colour diagram in the CIE 1931 obtained from the reflectance and calculated from the equation of the model proposed for 8 nm Cr-AAO-Al and 10 nm Au-AAO-Al nanostructures, respectively. The errors of *x* and *y* values were calculated using the propagation of uncertainties.

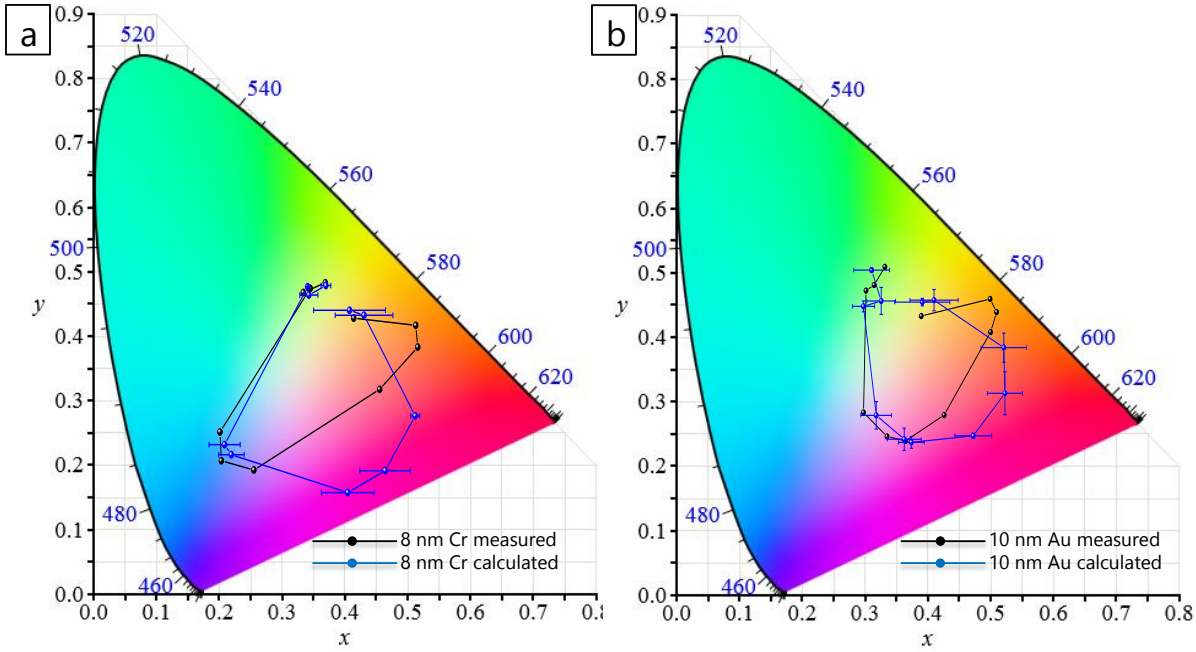


Figure 4. Representation of the colour diagram in the CIE 1931 (a) for 8 nm Cr-AAO-Al, and (b) for 10 nm Au-AAO-Al films; measured values are plotted in black and calculated values in blue.

The thickness, the *x* and *y* values measured from the reflectance, and the *x* and *y* values calculated using the proposed model for 8 nm Cr/AAO/Al and 10 nm Au/AAO/Al nanostructures are presented in Table S1. As can be seen in Figure 4 and Table S1, the observed colour is the same as the colour predicted using the model. A certain error is obtained, due to thickness measurement difficulties of the thin films, where the thickness error values were high. The *x* and *y* error values depend strongly on the thickness error as the x and y values depend on $\theta$ and $R(\theta)$. $\theta$ depends on the thickness, as shown in equations (2), (3), (S3) and (S4). The model fits better when 10 nm Au is deposited onto the AAO-Al films rather than when 8 nm Cr is sputtered onto these films. It should be noted that measuring the thickness of the thin films, as

well as obtaining accurate values is very difficult, due to the roughness and large surface area (2.5 $cm^2$ in diameter) of the AAO films. This can be seen in Figure S4 (supporting information) on the FE-SEM images of the cross-section of an AAO film after FIB cutting.

The *x* and *y* values calculated from the proposed model were plotted as a function of the *x* and *y* values from the reflectance measurements, in order to check the validity of the proposed model (see Figure S5a). In order to compare the proposed model in this study and the method using the wavelength of the maximum reflectance, the *x* and *y* values were calculated from the wavelength of the maximum reflectance and were plotted as a function of the *x* and *y* obtained from the reflectance (see Figure S5b). The slope and $R^2$ values, 0.94±0.09 and 0.82, respectively, were obtained by plotting the calculated *x* and *y* values as a function of the *x* and *y* values obtained from the reflectance measurements. However, when the *x* and *y* values from $\lambda_{max}$ were plotted as function of the *x* and *y* values from the reflectance, the slope and $R^2$ were 2.09±0.31 and 0.47, respectively. These values corroborate that the mathematic model proposed in this study is more accurate that other equations found in literature, which use wavelengths and not tristimulus values that describe a gamut of colours using CIElab 1931 colour space. This empirical model can be applied to any type of material and metals' thicknesses deposited on the surface of AAO-Al films, and can be extended to thicker AAO films considering more colours in the inner part of the colour diagram circle.

## Conclusions

In summary, 8 nm Cr-AAO-Al and 10/17.5/25 nm Au-AAO-Al nanostructures were fabricated by combining sputtering deposition and a two-step anodization process. The AAO films with different thicknesses (from 209 ± 12 nm to 380 ± 15 nm) were anodized and the *Yxy* values were obtained via reflectance measurements. A mathematic model, which describes a gamut of colours, was proposed using only the thickness and porosity of the AAO films. This model was defined for two different metals, i.e. Cr and Au, finding similar equations for both, as the porosity after the deposition of both metals onto the AAO-Al films was very similar. The proposed model can be used for porous templates with different morphological properties and metal layers deposited onto these templates. This study provides a simple mathematical model, which can be useful in different applications, such as wavelength absorbers, RGB display devices, as well as chemical or optical sensors.

## Methods

### *Fabrication of the AAO films*

Highly ordered anodic aluminium oxide (AAO) films were fabricated using a two-step anodization process [19] following the same conditions reported in previous manuscripts of our group[4, 17]. The anodization conditions used in this study were as followed: a 0.3 M oxalic acid electrolyte, applied potential of 40 V and temperature of 3 °C. Different thicknesses were obtained by applying different second anodization times. Different AAO films were anodized under the same conditions (same porosity and thickness) and the porosity of the films was changed by applying different chemical etching times (from 2 to 8 min) using a 5 wt.% of $H_3PO_4$ solution at 35 °C. In order to obtain different colours on the nanostructures, an 8 nm thin film of chromium was applied using Alliance-Concept DP 650 DC magnetron sputtering equipment and 25, 17.5 and 10 nm thin films of gold were deposited using Leica EM ACE600 sputtering equipment on top of the AAO films. For Au film, the sputtering pressure and intensity were $5 \cdot 10^{-2}$ mbar and 30 mA, respectively, and for the Cr film the sputtering pressure and power were $5 \cdot 10^{-3}$ mbar and 350 W, respectively. Metal-anodic aluminium oxide (AAO)-Al nanostructures were formed by depositing 25 nm/17.5nm/10nm of Au or 8 nm of Cr, AAO, and using mirror Al (which was obtained using an electropolishing process on Al foil) before the anodization process.

### *Characterization of AAO films*

Morphological characterisation was performed using field emission scanning electron microscopy (FE-SEM, Hitachi S-4800) with a 1.5 kV accelerating voltage. The thickness was obtained from cross-sectional images taken using a focused ion beam (FIB) instrument (TESCAN Lyra, Brno, Czech Republic) with a gallium source at 30 kV and 180-400 pA. 2 µm of platinum was deposited to protect the surface prior to the FIB cutting. FE-SEM images were taken in three different areas of the films and three different measurements were done. The thickness was calculated by averaging the nine measurements. Reflectance spectroscopy measurements on the AAO films were carried out using a PerkinElmer Lambda 900 UV-VIS spectrophotometer, ranging from 300 to 900 nm. *Yxy* values represent another colour model that describes luminance (*Y*) and chromaticity (*xy)* using the CIE 1931 colour space[12], which were obtained from the UV-Vis reflectance values of the nanostructures (Cr/Au-AAO-Al).

## AUTHOR INFORMATION

Corresponding Author:

*Email: cristina.vicente@csic.es.

ORDIC: 0000-0001-5708-6544

### Notes

The authors declare no competing financial interest.

## ACKNOWLEDGMENT

C.V.M. would like to acknowledge funding support from the Marie Curie Actions cofund program of the EU's Seventh Research Framework Program (FP7).

## REFERENCES

1. Kolle, M.; Salgard-Cunha, P. M.; Scherer, M. R. J.; Huang, F.; Vukusic, P.; Mahajan, S.; Baumberg, J. J.; Steiner, U. *Nat Nano* **2010**, *5* (7), 511-515, 10.1038/nnano.2010.101.
2. Kikuchi, T.; Nishinaga, O.; Natsui, S.; Suzuki, R. O. *Electrochimica Acta* **2015**, *156* (Supplement C), 235-243.
3. Ruiz-Clavijo, A.; Tsurimaki, Y.; Caballero-Calero, O.; Ni, G.; Chen, G.; Boriskina, S. V.; Martín-González, M. *ACS Photonics* **2018**, *5* (6), 2120-2128, Article.
4. Manzano, C. V.; Ramos, D.; Pethö, L.; Bürki, G.; Michler, J.; Philippe, L. *Journal of Physical Chemistry C* **2018**, *122* (1), 957-963, Article.
5. Oller, D.; Fernandes, G. E.; Siontas, S.; Xu, J.; Pacifici, D. *Materials Research Bulletin* **2016**, *83*, 556-562.
6. *28th IEEE International Conference on Micro Electro Mechanical Systems (MEMS)*, 18-22 Jan. 2015; 2015.
7. Guo, D.-L.; Fan, L.-X.; Wang, F.-H.; Huang, S.-Y.; Zou, X.-W. *The Journal of Physical Chemistry C* **2008**, *112* (46), 17952-17956.
8. Bae, K.; Lee, J.; Kang, G.; Yoo, D.-S.; Lee, C.-W.; Kim, K. *RSC Advances* **2015**, *5* (125), 103052-103059, 10.1039/C5RA17637A.
9. Pashchanka, M.; Yadav, S.; Cottre, T.; Schneider, J. J. *Nanoscale* **2014**, *6* (21), 12877-12883, 10.1039/C4NR03167A.
10. Wang, X.; Zhang, H.; Zhang, D.; Ma, Y.; Fecht, H. J.; Jiang, J. Z. *Microscopy Research and Technique* **2012**, *75* (5), 698-701.
11. Xue, J.; Zhou, Z.-K.; Wei, Z.; Su, R.; Lai, J.; Li, J.; Li, C.; Zhang, T.; Wang, X.-H. *Nature Communications* **2015**, *6*, 8906, Article.
12. Smith, T.; Guild, J. *Transactions of the Optical Society* **1931**, *33* (3), 73.
13. Choi, D.; Shin, C. K.; Yoon, D.; Chung, D. S.; Jin, Y. W.; Lee, L. P. *Nano Letters* **2014**, *14* (6), 3374-3381.
14. Xulongqi, W.; Dongxian, Z.; Haijun, Z.; Yi, M.; Jiang, J. Z. *Nanotechnology* **2011**, *22* (30), 305306.
15. Purves D, A. G., Fitzpatrick D, et al., . *Neuroscience. 2nd edition. Cones and Color Vision.* ; 2001.

16. Nielsch, K.; Choi, J.; Schwirn, K.; Wehrspohn, R. B.; Gösele, U. *Nano Letters* **2002**, *2* (7), 677-680, doi: 10.1021/nl025537k.
17. Manzano, C. V.; Best, J. P.; Schwiedrzik, J. J.; Cantarero, A.; Michler, J.; Philippe, L. *Journal of Materials Chemistry C* **2016**, *4* (32), 7658-7666, 10.1039/C6TC01904H.
18. Xu, Q.; Sun, H. Y.; Yang, Y. H.; Liu, L. H.; Li, Z. Y. *Applied Surface Science* **2011**, *258* (5), 1826-1830.
19. Masuda, H.; Fukuda, K. *Science* **1995**, *268* (5216), 1466-1468; Martín, J.; Manzano, C. V.; Caballero-Calero, O.; Martín-González, M. *ACS Applied Materials & Interfaces* **2013**, *5* (1), 72-79, doi: 10.1021/am3020718; Manzano, C. V.; Martín, J.; Martín-González, M. S. *Microporous and Mesoporous Materials* **2014**, *184* (0), 177-183.